THE JOURNAL OF PHYSICAL CHEMISTRY A

Article

pubs.acs.org/JPCA

Controlling S_2 Population in Cyanine Dyes Using Shaped Femtosecond Pulses

Muath Nairat,[†] Arkaprabha Konar,[†] Vadim V. Lozovoy,[†] Warren F. Beck,[†] G. J. Blanchard,[†] and Marcos Dantus*[,†,‡]

[†]Department of Chemistry, Michigan State University, East Lansing, Michigan 48824, United States

[‡]Department of Physics and Astronomy, Michigan State University, East Lansing, Michigan 48824, United States

Supporting Information

ABSTRACT: Fast population transfer from higher to lower excited states occurs via internal conversion (IC) and is the basis of Kasha's rule, which states that spontaneous emission takes place from the lowest excited state of the same multiplicity. Photonic control over IC is of interest because it would allow direct influence over intramolecular nonradiative decay processes occurring in condensed phase. Here we tracked the S_2 and S_1 fluorescence yield for different cyanine dyes in solution as a function of linear chirp. For the cyanine dyes with polar solvation response IR144 and *meso*-piperidine substituted IR806, increased S_2 emission was observed when using transform limited pulses, whereas chirped pulses led to increased S_1 emission. The nonpolar solvated cyanine IR806, on the other hand, did not show S_2 emission. A theoretical model, based on a nonperturbative solution of the equation of motion for the density matrix, is offered to explain and simulate the anomalous chirp dependence. Our findings, which depend on pulse properties beyond peak intensity, offer a photonic method to control S_2 population thereby opening the door for the exploration of photochemical processes initiated from higher excited states.

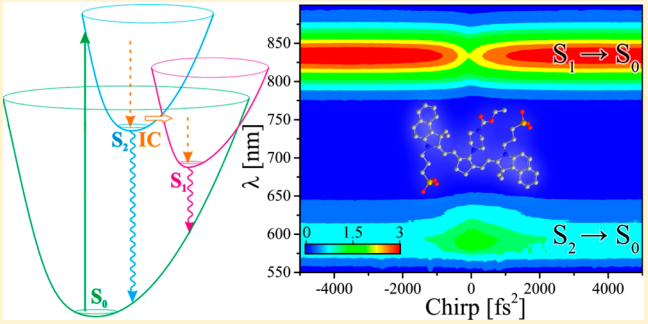

INTRODUCTION

Kasha's rule is one of the fundamental phenomena governing the photochemistry and photophysics of molecules in condensed phase. It states that following excitation to higher electronic excited states, spontaneous emission occurs from the lowest electronic excited state, independent of the photon energy used during the excitation process.[1] The basis for this rule is that the rates of nonradiative processes such as, internal conversion (IC), intersystem crossing (ISC) and vibrational relaxation from higher excited states are much faster than the spontaneous radiative decay rate of that excited state.[2] Some compounds, such as azulenes, aromatic acenes, thioketones, and polyenes have been observed to violate Kasha's rule and exhibit fluorescence from higher excited states simultaneously along with the fluorescence from the lowest excited state.[2]

Photonic control of intramolecular nonradiative decay pathways opens up the possibility of utilizing higher excited states to manipulate the final product distribution of photo-induced reactions,[3] design optoelectronic switches[4] and utilize more efficient charge transfer events.[5] It has been reported that by controlling the properties of the molecular environment, such as pH and viscosity, the dual emission behavior noted above was affected due to changes in the excited state intramolecular proton/charge transfer.[6,7] Structural changes such as the carbon substitution position of organometallic complexes play a key role in changing nonradiative metal-to-ligand charge transfer state that leads to the production of dual emissive states.[8] Here, as part of our efforts toward understanding and controlling laser-matter interactions,[9] we explore photonic control over Kasha's rule with the goal of significantly enhancing emission from a higher (S_2) electronic state.

Cyanines are a class of polymethine dyes structurally related to protonated Schiff bases, carotenoids, and other conjugated polyenes. Some are approved for photodynamic therapy and bioimaging;[10] their backbone consists of an odd number of conjugated $2p_z$ orbitals that results in a S_0-S_1 transition in the visible or near-IR region. The large S_2-S_1 energy gap ranges from 0.6 to 1 eV, and leads to comparatively weak coupling between the two excited states and a slowing of the IC rates according to the energy gap law, which states that IC rate decreases exponentially with increasing energy separation.[11] Cyanine dyes exhibit dual fluorescence when excited directly to the S_2 state.[12−15] The fluorescence quantum yield and lifetime of the S_2 state for cyanine dyes has been shown to increase with solvent viscosity.[16]

The broad and essentially featureless absorption spectra of polyatomic molecules in condensed phase poses a challenge for photonic control strategies especially when compared to the

Received: February 23, 2016
Revised: March 1, 2016
Published: March 3, 2016

DOI: 10.1021/acs.jpca.6b01835
J. Phys. Chem. A 2016, 120, 1876−1885

spectra of isolated small molecules for which energy levels are sharp and well-defined. Spectral broadening due to spectral congestion and inhomogeneous and homogeneous broadening prevent one from mapping potential energy surfaces and finding gateways responsible for IC, ISC, and barriers to isomerization. Linear chirp, one of the simplest forms of pulse shaping and results in a carrier frequency sweep from higher to lower frequencies (positive chirp) or the reverse sweep (negative chirp), has been used previously to control population and hence fluorescence yields of large molecules in solution.[17,18] Chirped pulses have also been used to control the yield of a desired photoproduct[19,20] and population transfer in fluorescent proteins.[21] The chirp dependence of molecular fluorescence from S_1 states has been explained theoretically.[18,22−26] Control with more complex pulse shapes resulting from closed loop optimization have been used to control processes related to solar energy capture, suppression of radiationless transitions, and photoisomerization; the effect of shaped pulses on the yields of photoproducts has been demonstrated experimentally[27−33] and theoretically.[34−37] These efforts have been reviewed in the past.[9,38,39] While some of the work referenced here include excitation to S_2,[27,36] robust control of S_2 to S_1 IC using shaped pulses has not been reported. Here we explore control of S_2 fluorescence yield using chirp following direct S_2 excitation. In our experiments, we monitor fluorescence from both S_2 and S_1 states, as a function of chirp for different cyanine dyes.

EXPERIMENTAL METHODS

Laser and Pulse Shaper. The experimental setup shown in Figure 1 uses a noncollinear optical parametric amplifier (NOPA, Spectra-Physics Spirit NOPA-3H) as a source of tunable femtosecond pulses. The NOPA is pumped by an amplified direct diode-pumped Yb laser (Spectra-Physics Spirit 1040−4) which delivers 1040 nm pulses at a 100 kHz repetition rate with pulse energy of 40 μJ. The NOPA has a built-in third harmonic generator that is used to pump the white-light continuum seed pulses in order to generate visible wavelengths tunable from 500 to 750 nm. For the current experiments, we used pulses centered at 517, 540, and 545 nm. The NOPA pulses were compressed and shaped using a femtoJock (Biophotonic Solutions Inc. USA) phase and amplitude pulse shaper using the multiphoton intrapulse interference phase scan (MIIPS) method.[40,41] The pulse durations ranged from 13 to 16 fs depending on the excitation wavelength.

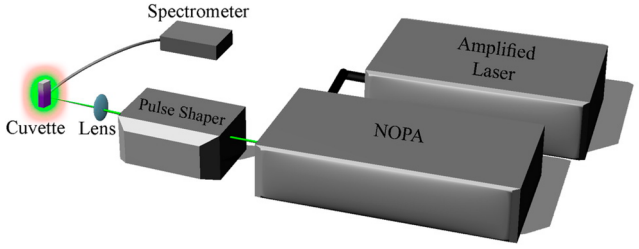

Figure 1. Experimental setup. The output of the NOPA was phase and amplitude shaped using MIIPS femtoJock pulse shaper and then was focused on the cyanine dye in a 2 mm path length cuvette, the fluorescence signal was detected directly at a right angle using a fiber-coupled compact spectrometer.

Fluorescence Excitation and Detection. The compressed pulses were focused with a 10 cm focal length lens onto a cuvette having a 2 mm path length. Second order dispersion caused by the cuvette wall on the incident side of the beam was accounted for when compressing the pulses using the MIIPS procedure with the pulse shaper. Solvent introduced dispersion, which is about 60 fs^2/mm at our working wavelength,[42] was minimized by collecting the signal at a right angle near the entrance cuvette window with a multimode optical fiber, with 25 degree acceptance angle, placed in contact with the cuvette. Chirp phase masks of the form $\phi(\omega) = 0.5\phi''(\omega - \omega_0)^2$, where ϕ'' is the quadratic phase, were applied using the pulse shaper. The chirp scan was conducted by varying the quadratic phase from negative to positive 5000 fs^2. Quadratic phase on the transform limited (TL) pulse stretches it to longer durations according to $\tau/\tau_{TL} = \sqrt{1 + (4 \ln 2)^2(\phi''/\tau_{TL}^2)^2}$. Laser fluence dependence measurements were carried out by changing the amplitude mask in the pulse shaper while ensuring retention of the desired phase mask. Chirp scan experiments were conducted with pulse energies of 31 nJ ∼ 1.1 mJ/cm^2 laser fluence for IR144 and 18 nJ ∼ 0.65 mJ/cm^2 for *meso*-piperidine-IR806 (*m*Pi-IR806), while simultaneously detecting the fluorescence from S_1 and S_2 excited states. The fluorescence collected by the optical fiber was detected using a compact spectrometer (Ocean Optics USB4000).

Samples. The experiments were carried out on three cyanine dyes: 50 μM IR144 (Exciton) dissolved in methanol, 50 μM IR806 (Sigma-Aldrich) dissolved in methanol, and 50 μM *m*Pi-IR806 dissolved in propanol. The chemical structures of the cyanine dyes studied here IR806, IR144 and *m*Pi-IR806 are shown in Scheme 1. *m*Pi-IR806 was prepared using a published procedure[43] using IR806 (0.02 mmol) and piperidine (0.1 mmol), which were stirred at room temperature in DMF for 16 h. NMR shifts confirming the identity of *m*Pi-IR806 are provided in the Supporting Information.

Scheme 1. Structures of (a) IR806, (b) IR144, and (c) *m*Pi-IR806

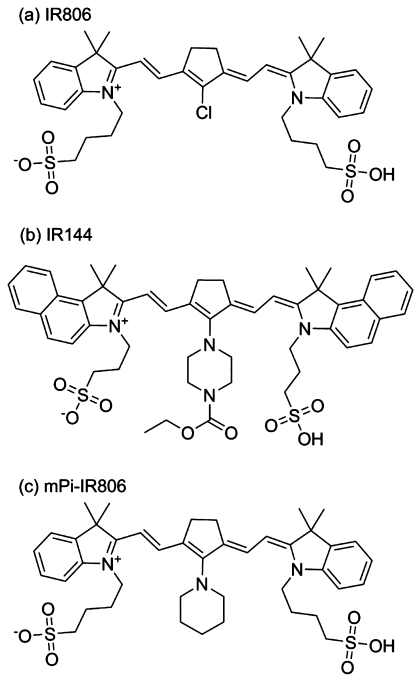

DOI: 10.1021/acs.jpca.6b01835
J. Phys. Chem. A 2016, 120, 1876−1885

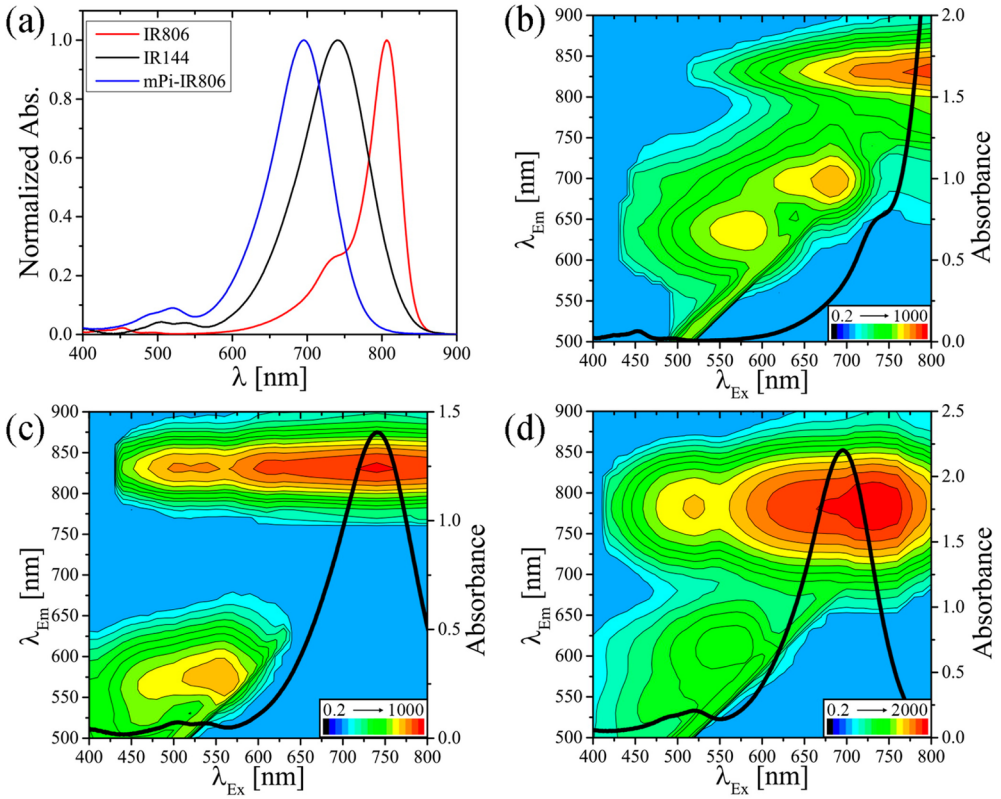

Figure 2. (a) Absorption spectra for the three cyanine-dyes in Scheme 1. Two-dimensional fluorescence excitation−emission spectra for (b) IR806, (c) IR144, and (d) *m*Pi-IR806. Contour lines are plotted on a logarithmic scale. The absorption spectrum (black line) for each dye is superimposed on the excitation axis.

Table 1. Absorption Maxima, Fluorescence Maxima, Stokes Shifts, and Fwhm of the Absorption and the Emission Spectra of the S_1 State for IR806, IR144, and *m*Pi-IR806[a]

	IR806 (methanol)	IR144 (methanol)	*m*Pi-IR806 (propanol)
Absorption maxima (cm^{-1})	12407 (806 nm)	13514 (740 nm)	14368 (696 nm)
Fluorescence maxima (cm^{-1})	11825 (845 nm)	11862 (843 nm)	12723 (786 nm)
S_1−S_0 Stokes shift (cm^{-1})	582	1652	1645
Absorption fwhm (cm^{-1})	778	1988	1935
Fluorescence fwhm (cm^{-1})	489	974	981

[a] S_1−S_0 Stokes shift measured as the difference between the absorption and fluorescence spectra maxima.

RESULTS

Steady State Spectroscopy. As in many other symmetrical cyanine dyes, the $\pi \rightarrow \pi^*$ transition in IR806 occurs without a significant change in the permanent dipole moment.[44−47] In IR144 and *m*Pi-IR806, however, there is a significant change in the permanent dipole moment associated with the optical excitation due to the addition of the 1-piperazinecarboxylate and piperidine groups, respectively, in conjugation with the main polyene backbone. This coupling contributes in producing a symmetrical ground state resonance structure that does not contribute to the antisymmetric excited state structure, resulting in a dipole moment change upon S_1 electronic excitation and triggering a polar solvation response.[45]

The steady state absorption spectra of IR806, IR144 (both dissolved in methanol) and *m*Pi-IR806 (dissolved in propanol) are shown in Figure 2a. The spectrum from the nonpolar solvated dye IR806 has in addition to a maxima at 806 nm, a shoulder at ca. 735 nm, a feature that is very common in the absorption spectra of cyanine dyes.[44,46,47] The polar solvated dyes, IR144 and *m*Pi-IR806, lack the vibronic feature and possess wider absorption spectra, with λ_{max} = 740 and 696 nm, respectively. Both, IR144 and *m*Pi-IR806 absorption spectra show small peaks with λ_{max} = 540 and 521 nm with cross sections of ca. 1.7 × 10^{-18} cm^2 and 3.6 × 10^{-18} cm^2, respectively. The absorption maxima, fluorescence maxima, Stokes shifts and full width at half maxima (fwhm) of the absorption and the fluorescence spectra from the S_1 state of the three dyes are presented in Table 1.

Two-dimensional fluorescence excitation−emission spectra for the three dyes help discern the presence of emission bands at higher energies as shown in Figure 2b−d. The absorption spectrum for each dye is superimposed on the excitation axis. The higher energy emission bands originate from the higher S_2 state or a structurally rearranged intramolecular charge transfer (CT) state within the S_1 manifold.[48] For IR806, higher energy emissions with maxima at 700 and 637 nm originate from the blue edge of the vibronic absorption band of the S_1 state and not from the S_2 state. This observation was further confirmed from fluorescence excitation spectra obtained when detecting these high-energy emissions (Figure S1, Supporting Informa-

DOI: 10.1021/acs.jpca.6b01835
J. Phys. Chem. A 2016, 120, 1876−1885

tion), and has been observed to occur from nonpolar solvated cyanines.[49] The assignment was further confirmed by the observed reduced fluorescence yield observed as a function of increased solvent viscosity (Figure S2).

The spectroscopy and photophysics of the S_1 excited state of the cyanine dye IR144 have been discussed in the literature.[45,50−52] However, little is known about the dynamics of higher excited state(s) of this dye and its close analogue *m*Pi-IR806. The two-dimensional excitation-fluorescence spectra (Figure 2c-d) for the two dyes reveal higher emission bands that arise mainly from absorption bands with λ_{max} = 540 and 521 nm for IR144 and *m*Pi-IR806, respectively. Correlation between the S_2 absorption and excitation spectra was observed for the emissions with maxima at ca. 588 nm for IR144 and ca. 557 nm for *m*Pi-IR806 (Figure S3). Unlike IR806, the high-energy emission bands from IR144 and *m*Pi-IR806 were found to increase with solvent viscosity (Figure S4), in agreement with previous studies on cyanines S_2 fluorescence that attributed this finding to the need for out-of-planar motion to couple S_2 to S_1 energy transfer.[16] Fluorescence lifetime measurements for IR144 and *m*Pi-IR806 S_2 and S_1 states are shown in Figure S5 and S6.

Chirp Studies on the S_2 State of IR144 and mPi-IR806. Fluorescence yield dependence on chirp experiments on IR144 were carried out using 16 fs laser pulses centered at 545 nm that match the S_2 absorption profile of IR144 to excite the sample while simultaneously detecting the resolved fluorescence signal from the S_1 and S_2 states using the same spectrometer. The same approach was followed with *m*Pi-IR806 using 13 fs pulses centered at 517 nm matching the S_2 absorption profile. The fluorescence spectra for IR144 using the aforementioned laser spectrum produced two peaks with maxima at 588 and 843 nm that are from S_2 and S_1 states, respectively (Figure S7a). While the *m*Pi-IR806 fluorescence peak maxima were at 558 and 786 nm, which are from S_2 and S_1 states, respectively (Figure S7b). It is worth noting that using the 517 nm-centered pulses, *m*Pi-IR806 fluorescence with maxima at 558 nm was mainly from the S_2 state without much involvement of the emission at 614 nm (see Figure 2d).

The observed fluorescence yields from S_2 and S_1 were found to be dependent on chirp as shown in Figure 3. No spectral shifts were observed as a function of chirp (Figure 3 inset). The enhancement of the S_2 fluorescence yield observed for TL pulses corresponds to a concomitant depletion of emission from the S_1 state. The anomalous S_2 fluorescence as a function of chirp was found to differ drastically from the typical "chirp effect" dependence in general and in particular when exciting the IR144 S_1 state.[18,26,53,54] By typical chirp effect, we refer to the observation of reduced fluorescence yield when using negatively chirped pulses; the reduced yield caused by stimulated emission induced by the redder frequencies following the bluer frequencies. In a typical chirp experiment, maximum fluorescence yield is observed for positively chirped pulses. Clearly, S_2 excitation with chirped pulses does not agree with previous findings and leads to anomalous chirp dependence.

Chirps greater than 3000 fs^2 reduce S_2 fluorescence by about 42% and 13% compared to what is obtained using TL pulses for IR144 and *m*Pi-IR806, respectively. The chirp dependence is asymmetric, with greater depletion for negative values especially for *m*Pi-IR806. The asymmetry is observed at laser fluence higher than ~0.5 mJ/cm^2 (see Figure 4, parts b and d). Lower emission from the resonant state (here S_2) would be expected

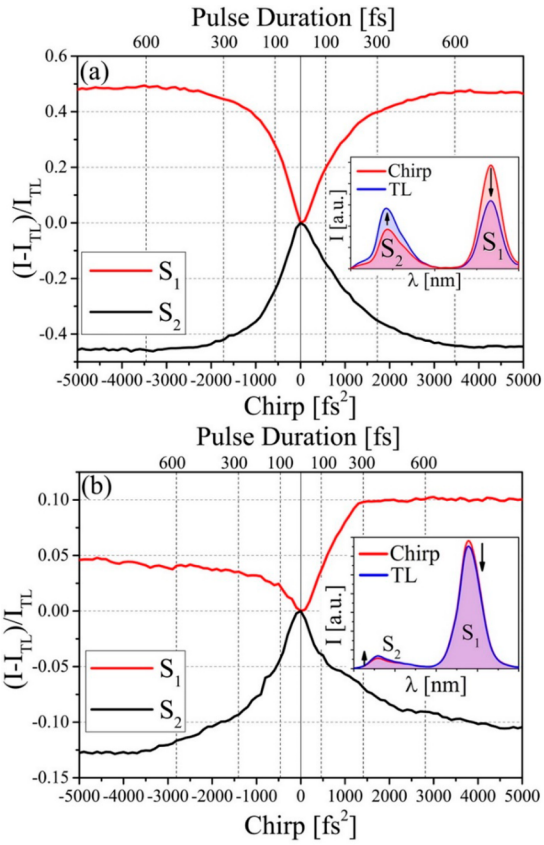

Figure 3. Integrated fluorescence intensity from S_1 (red) and S_2 (black) states as a function of linear chirp for (a) IR144 and (b) *m*Pi-IR806, top axis shows the corresponding chirped pulse duration. TL pulses lead to greater S_2 fluorescence, while chirped pulses lead to greater S_1 fluorescence. A greater degree of asymmetry between positive and negative chirp values is observed for *m*Pi-IR806. Inset: S_1 and S_2 emission spectra when excited by TL (blue) and chirped (red) pulses.

with negatively chirped pulses, which deplete the excited state population before intramolecular vibrational redistribution and fluorescence occurs by tracking the excited-state wavepacket's motion from the Franck−Condon (FC) geometry to lower energy.[26] The degree of symmetry with respect to chirp is important because it establishes that the dynamics are sensitive to the order in which different frequencies arrive. An asymmetric response can be observed when dynamics occur on a similar time scale to the excitation laser pulse.[55] The slightly asymmetric S_2 fluorescence dependence observed implies that wavepacket motion out of the FC region occurs on a time scale comparable with the pulse duration.

From the results in Figure 3, we find that the fluorescence yield from the S_2 state is greater when excited using TL pulses and lower for chirped pulses. What is unexpected and surprising is that the yield of S_1 fluorescence does not mimic the yield of S_2 fluorescence, given that most of the S_1 population is attained via IC from S_2. When comparing the chirp dependence of the S_2 and S_1 states in Figure 3 for IR144, it can be seen that changes in the fluorescence yields from the two states are anticorrelated; i.e. TL pulses maximize S_2 and minimize S_1 population. In other words, the S_2 fluorescence enhancement occurs at the expense of IC to S_1. The same is observed for *m*Pi-IR806 when comparing the fluorescence yield from both states using TL and positive chirp. Differences between IR144

DOI: 10.1021/acs.jpca.6b01835
J. Phys. Chem. A 2016, 120, 1876−1885

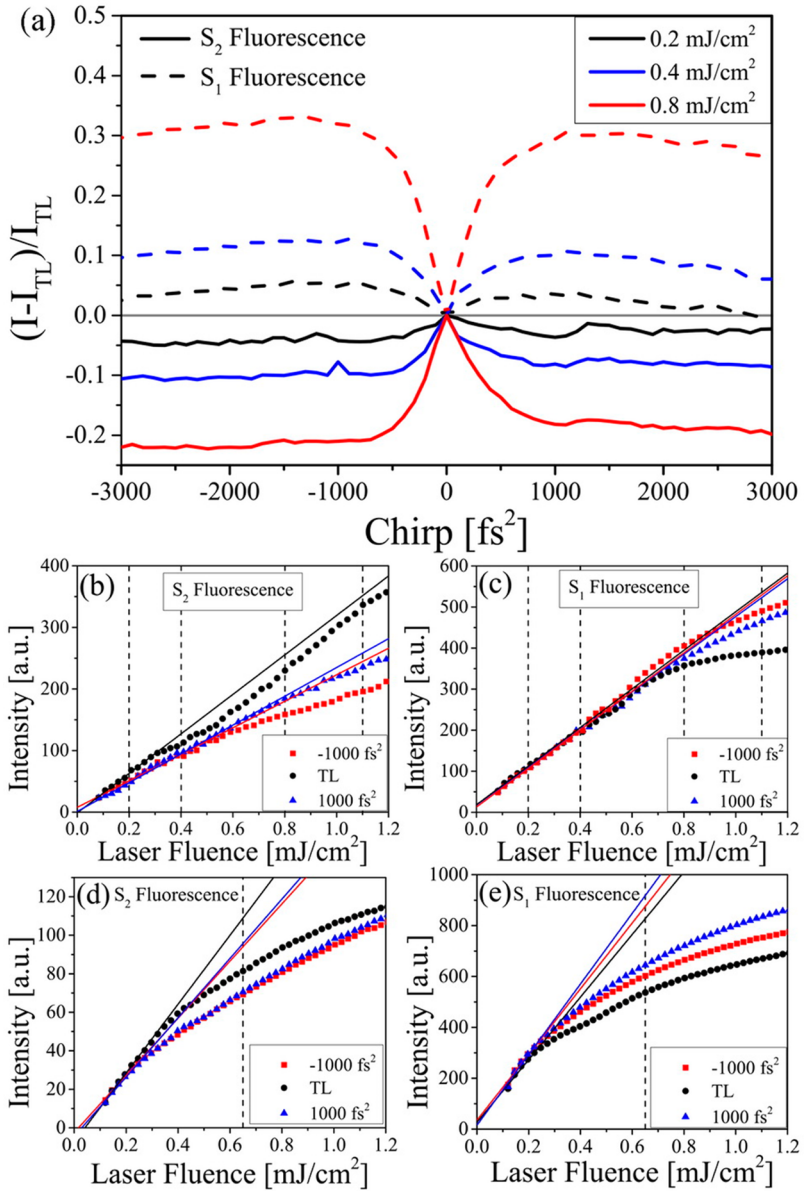

Figure 4. (a) IR144 S_2 (solid lines) and S_1 (dashed lines) fluorescence yield as a function of chirp at various laser fluence values. Fluorescence intensity dependence as a function of laser fluence for IR144 from (b) S_2 and (c) S_1 states using TL (black), negatively (red) and positively (blue) chirped 1000 fs^2 pulses. Fluorescence intensity dependence as a function of laser fluence for *m*Pi-IR806 from (d) S_2 and (e) S_1 states using TL (black), negatively (red) and positively (blue) chirped 1000 fs^2 pulses. The vertical lines indicate the laser fluence values at which the chirp scans were carried out. Linear fitting for the fluorescence yield at low laser fluence (0.1−0.25 mJ/cm^2) is shown as a guide to discern where nonlinear fluence dependence becomes important.

and *m*Pi-IR806 arise from the fact that excitation is not exclusive to the S_2 state. Therefore, the chirp trace for the S_1 fluorescence of *m*Pi-IR806 is a result of two components; (i) direct S_1 excitation evidenced by the depleted fluorescence on the negative side, (ii) IC from S_2 evidenced by the fluorescence depletion using TL pulses. In both cases, the excitation pulse, which prepares the initial wave packet on the S_2 surface, controls IC to the lower excited state.

Fluorescence yield experiments were repeated for IR144 at lower laser fluences, as shown in Figure 4a. The chirp dependence found at lower fluences, where fluorescence yield is linear with laser intensity, is similar to what was found at higher fluences and shown in Figure 3a. Fluorescence yield as a function of laser fluence was recorded using TL, negatively and positively (1000 fs^2) chirped pulses for IR144 (Figure 4, parts b and c) and *m*Pi-IR806 (Figure 4, parts d and e). For both molecules, linear dependence of fluorescence intensity is observed at lower laser fluence for both S_1 and S_2 states. Note that for all laser fluences and for both molecules S_2 fluorescence is greater for TL pulses compared to chirped ones. Conversely, S_1 fluorescence is greater for chirped pulses as opposed to TL pulses. These differences only increase with intensity.

No S_2 fluorescence was observed for IR806. This absence may be related to the nonpolar solvation nature of this cyanine dye. Nevertheless, we see the absence of S_2 fluorescence to serve as an important control, albeit negative, for our research. The S_1 fluorescence yield as a function of chirp for IR806 (Figure S8) shows minimum fluorescence yield for negative chirps and maximum for positive chirps, what we have earlier

DOI: 10.1021/acs.jpca.6b01835
J. Phys. Chem. A 2016, 120, 1876−1885

termed typical chirp dependence. We ascribe this behavior to the nonpolar nature of the S_1 state in IR806.

Theoretical Modeling. A full simulation of the present experiment, including *ab intio* calculations of the relevant ground and excited states in the presence of solvent and the intense laser fields, are presently out of our reach. There is sufficient information about the S_1 and S_0 potential energy surfaces to determine that initial dynamics following excitation in S_1 is along the so-called bond-length alternation (BLA) coordinates.[56,57] In the longer cyanines ($n \geq 5$), a significant barrier on the S_1 surface divides planar and twisted conformations of the polyene backbone. Beyond the barrier, the system descends steeply along torsional gradients. A CI between S_1 and S_0 is responsible for nonradiative decay from S_1. For IR144 and *m*IR806, the large S_1−S_0 Stokes shift and the significant increase in S_2−S_0 fluorescence with increased viscosity leads one to expect that S_2 has a more planar geometry than S_1. A simplified schematic representation of the three singlet states inspired by Jortner's gap law strong coupling case,[58] for S_2 emission from molecules with internal conversion is shown in Figure 5. In addition, we depict an effective model with the minimum number of energy levels that can help explain our findings.

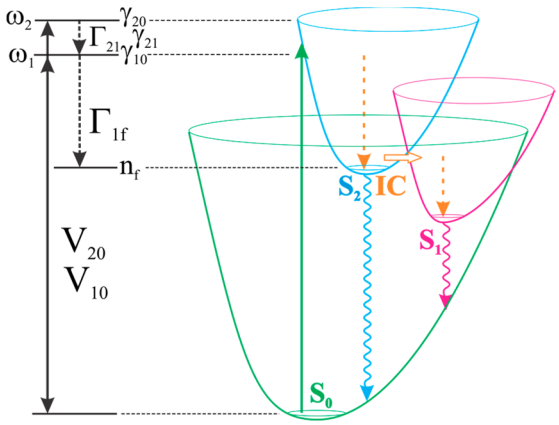

Figure 5. Simplified schematic of S_0, S_1, and S_2 energy levels considered in our model. (Left) Four level model used for our calculations, consists of the ground state and 3 levels in the S_2 excited state.ω_0 is the laser frequency, ω_1 and ω_2 are frequencies of the two levels in S_2 that interact with the laser. n_f is the population reaching the bottom of S_2, note this state is outside the laser spectrum, V is the transition dipole dependent laser interaction, Γ is the relaxation rate, γ is the dephasing rate. (Right) Schematic representation of the three lower singlet states of cyanine molecules plotted as a function of spatial coordinates involving twisting from the planar ground state configuration and bond lengthening. Internal conversion (IC) to S_1 requires twisting. The IC from S_1 to S_0 expected at a torsion angle of 90° is not indicated.

The relevant energy levels consist of a ground state level and three levels representing the S_2 state. The upper two levels (ω_1 and ω_2) are consistent with the S_2 absorption spectrum features while the lowest energy level (n_f) corresponding to the bottom of the S_2 state, which fluoresces at wavelengths far from the excitation laser and is therefore dark to the excitation laser pulse. The laser frequency ω_0 was set to interact with the higher two levels ω_1 and ω_2 while both levels were set to relax irreversibly. Our goal is first to solve for the population in (n_f) as a function of chirp. Then, because S_1 is populated via IC only from the upper levels but not from the lowest level, consistent with the observation of S_2 fluorescence, the total excited population from the ground state ends as population in either S_2 or S_1. Therefore, S_1 population equals $(1 - S_2)$ which has an inverse dependence on chirp compared to S_2. Our experiments are performed in a regime where fluorescence from S_2 has very slight saturation for TL or chirped pulse excitation (Figure 4), therefore, our model should be able to take into account nonlinear optical laser-molecule interactions. We used a nonperturbative solution of the equation of motion for the density matrix eq 1 and eq 2[59] to describe the system in the presence of the field

$$\frac{d\rho_{aa}}{dt} = -\frac{i}{\hbar}\sum_{v}(V_{av}\rho_{va} - \rho_{av}V_{va}) + \sum_{Eb>Ea}\Gamma_{ab}\rho_{bb} - \sum_{Ea>Eb}\Gamma_{ba}\rho_{aa} \quad (1)$$

$$\frac{d\rho_{ab}}{dt} = -i(\omega_a - \omega_b)\rho_{ab} - \frac{i}{\hbar}\sum_{v}(V_{av}\rho_{vb} - \rho_{av}V_{vb}) - \gamma_{ab}\rho_{ab} \quad (2)$$

where V is the transition dipole, a and b represent the levels in the model, and ρ_{aa} and ρ_{ab} are the diagonal and the off diagonal elements of the density matrix which represent the populations and coherences between the levels, respectively. The coherence-dephasing rate is $\gamma_{ab} = {}^1/_2(\Gamma_a + \Gamma_b)$, where Γ_a and Γ_b are the relaxation rates. The dipole moment matrix interaction with the chirped pulses is represented by eq 3.

$$V_{ab}(t) = \mu_{ab}E_0\sqrt{\frac{\tau_0^2}{\tau_0^2 - i\phi''}}\exp\left[-\frac{1}{2}\frac{t^2}{\tau_0^2 - i\phi''}\right] \quad (3)$$

where μ_{ab} is the dipole moment matrix element, τ_0 is the TL pulse duration, and ϕ'' is the chirp value.

When solving the system of differential equations numerically for the population in the lowest level (n_f), the best match with the experimental observations was found when we set ω_1 to be resonant with the laser frequency while ω_2 was set to the vertical transition frequency obtained from Lorentzian peak deconvolution of the experimental S_2 absorption band. The transition dipole moment matrix element μ_{ab} for each level was set as the square root of the relative strength of each deconvoluted peak from the S_2 absorption band, given that the absorbance is directly proportional to the square of the transition dipole moment. The relaxation time $\tau_2 = 1/\Gamma_{21}$ from ω_2 to ω_1 consistent with our simulation was found to occur on a very fast time scale of about 10 and 5 fs for IR144 and *m*Pi-IR806, respectively. Such value is in close proximity to reported IR144 three-pulse photon-echo peak shift component from the S_1 state that arise due to backbone stretching intramolecular vibrations.[50] The other relaxation component$\tau_1 = 1/\Gamma_{1f}$, which is from ω_1 to the final emitting level n_f was about 100 and 500 fs for IR144 and *m*Pi-IR806, respectively. These slower dynamics presumably involve torsion. Results from the simulations for the dependence of the final S_2 population and the S_1 population calculated as $S_1 = 1 - S_2$, are shown for IR144 (Figure 6a) and *m*Pi-IR806 (Figure 6b). The calculated S_1 population for *m*Pi-IR806 as $S_1 = 1 - S_2$ only represents IC from S_2, therefore we have also added S_1 population via direct S_1 excitation to match the experimental results. Direct S_1 population was carried out using a similar previous model that describes the S_1 chirp effect.[26] The S_1 level calculations were performed for a three level model consisting of one

DOI: 10.1021/acs.jpca.6b01835
J. Phys. Chem. A 2016, 120, 1876−1885

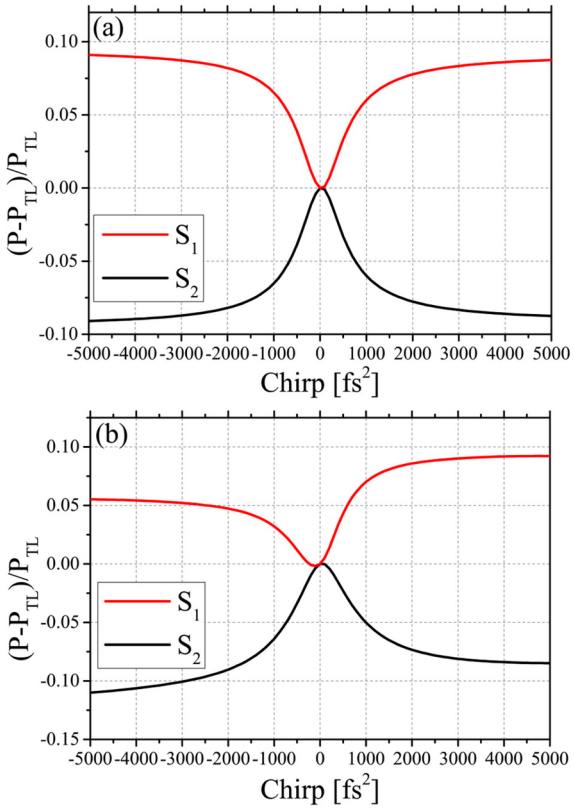

Figure 6. Theoretical simulations for S_2 state (black) and S_1 state (red) population as a function chirp for (a) IR144 and (b) *m*Pi-IR806.

ground level representing the ground state and two excited levels representing high-energy vibrational levels in the S_1 state. The laser field was set to interact equally with the two excited levels and the high level was set to relax on a 10 fs time scale to the lower level. The model was successful in reproducing the typical S_1 chirp effect as population depletion using negatively chirped pulses. The final *m*Pi-IR806 S_1 population trace shown in Figure 6b is a linear combination of 25% from direct S_1 interaction and 75% via IC from S_2.

From the reduced theoretical model, we find a set of conditions consistent with our experimental findings. TL pulses result in a larger population in the bottom of the S_2 potential than chirped pulses. This would imply that IC from S_2 to S_1, presumably through a conical intersection, occurs before the wave packet reaches the lowest point on the potential energy surface of S_2. This observation is consistent with the presence of S_2 fluorescence.

DISCUSSION

Interpretation of our experimental findings requires that we establish what is known and limit the number of processes to be considered to the fewest possible. The higher energy emission from the polar solvated dyes (IR144 and *m*Pi-IR806) originates from the S_2 state. On the basis of the hundreds of picoseconds fluorescence lifetimes of the S_2 state for IR144 and *m*Pi-IR806, we surmise that population that reaches the bottom of the S_2 potential, which is displaced in energy and in space from the FC region, is trapped by a barrier; *i.e.*, IC to S_1 slows dramatically. The barrier is likely to be the known polyene conjugation-length dependent transition state barrier, similar to that on the S_1 potential energy surface, which separates the planar FC region from that of twisted conformations, where a conical intersection with the ground state, S_0, is located.[57,60,61] However, this barrier is located on the S_2 surface and separates the FC from the conical intersection with the S_1 surface. These observations are further confirmed by enhanced S_2 emission as a function of increased solvent viscosity for both IR144 and *m*Pi-IR806. The observed enhancement of S_2 fluorescence for TL pulses becomes more pronounced as laser intensity increases. Our findings imply that chirped pulses create wave packets that more efficiently cross to S_1; this process is in dynamic competition with energy relaxation, which brings the population to the bottom of the S_2 potential well, where IC to S_1 is inefficient. From our theory and numerical calculations we find that IC must take place before energy relaxation, and dephasing must be very fast, <20 fs (TL pulse duration), and competes with vibrational relaxation and wave packet motion.

Two possible mechanisms for our experimental findings are considered. First, we suggest a mechanism based purely on first-order wave packet preparation. It is likely that TL pulse excitation creates a compact wave packet that is less efficient at crossing from S_2 to S_1 at short times than a diffuse wave packet, which better access the region where the S_2 and S_1 potential surfaces interact. Second, because TL pulse excitation is likely to drive more strongly double quantum excitations to a higher state S_n, cycling between the S_n and S_2 states would be expected to confine wave packets near to the S_2 planar minimum and suppress IC.[62−66] Similarly, TL pulse excitation strongly drives cycling between the S_2 and S_0 surfaces and limits IC accordingly.

The first mechanism is consistent with our observations because to some extent the chirp dependence is independent of laser intensity (as shown in Figure 4). We find that the fluorescence yield of S_2 is lower for chirped pulses than for TL pulses at all laser intensities, and fluorescence yield of S_1 is higher for chirped than for TL pulses (see Figure 4). The theory model offered here did not take into account calculation of FC factors of IC for wave packets created by TL or chirped pulses. The second mechanisms, whereby the laser strongly couples two or more states, is consistent with our finding that laser intensity caused a greater difference in the final state populations. While there is no reason *a priori* why excitation to higher excited states would preferentially end in S_2 rather than S_1, laser driven transitions between two states have been considered as means to alter vibrational relaxation dynamics[67] and to potentially cause population dependent dynamics.[68]

The exact photophysical process that leads to the observed control over IC is difficult to determine given the complexity of the systems. The Hamiltonian of each system has multiple dimensions and the location of a conical intersection between S_1 and S_2 has not been determined. Our observations, however, show photonic control over the higher excited state fluorescence in cyanine dyes. It is likely that the actual mechanism involves both of the proposed mechanisms. The degree of control exerted over S_2 population can be harnessed to explore the role of higher excited states in photochemical processes such as photosynthesis, especially in carotenoids where the first optically active state is a higher excited state that undergoes rapid IC to S_1.[69] We are working on more sophisticated theoretical models and numerical simulations. We hope the results presented here inspire future experiments and theoretical work.

DOI: 10.1021/acs.jpca.6b01835
J. Phys. Chem. A 2016, 120, 1876−1885

CONCLUSION

Control over internal conversion from S_2 to S_1 of the cyanine dyes IR144 and *m*Pi-IR806 has been achieved by phase control over the excitation pulses that prepare the initial population in the upper excited state. We found anomalous chirp dependence, whereby TL pulses cause a greater population in the excited state than chirped pulses. Furthermore, we find internal conversion to S_1 is not proportional to the total initial population but instead it is inversely proportional. The experimental results were successfully simulated using the equation of motion for the density matrix for a four level system. Under strong field interaction, TL pulses were more efficient in directing the population to the bottom of S_2 from which direct fluorescence occurs rather than IC to the S_1 state.

ASSOCIATED CONTENT

Supporting Information

The Supporting Information is available free of charge on the ACS Publications website at DOI: 10.1021/acs.jpca.6b01835.

Proton-NMR of *m*Pi-IR806, excitation spectra for the higher energy emission bands, fluorescence spectra obtained for different viscosities, fluorescence lifetime measurements, and IR806 chirp measurements (PDF)

AUTHOR INFORMATION

Corresponding Author

*(M.D.) E-mail: dantus@msu.edu. Telephone: +1 (517) 355-9715 x 314.

Notes

The authors declare no competing financial interests.

ACKNOWLEDGMENTS

This material is based upon work supported by the National Science Foundation under Grant CHE-1464807. Work in the Beck laboratory was supported by the Photosynthetic Systems program of Chemical Sciences, Geosciences and Biosciences Division, Office of Basic Energy Sciences, Office of Science, U.S. Department of Energy, under Award Number DE-SC0010847. M.D. and W.F.B. acknowledge support for the laser instrumentation from the Office of the Vice President of Research and Graduate Studies at MSU. We thank Dr. Rachel Glenn, Prof. Benjamin Levine, and Yinan Shu for useful discussions, Yousef Atoum for his help in running the simulations, Kedar Baryal for his help in the preparation of *m*Pi-IR806, and Elena Bongiovanni for help proof reading the manuscript.

REFERENCES

(1) Kasha, M. Characterization of Electronic Transitions in Complex Molecules. *Discuss. Faraday Soc.* **1950**, *9*, 14−19.

(2) Itoh, T. Fluorescence and Phosphorescence from Higher Excited States of Organic Molecules. *Chem. Rev.* **2012**, *112*, 4541−4568.

(3) Petersson, J.; Eklund, M.; Davidsson, J.; Hammarström, L. Variation of Excitation Energy Influences the Product Distribution of a Two-Step Electron Transfer: S2 vs S1 Electron Transfer in a Zn(II)porphyrin−Viologen Complex. *J. Am. Chem. Soc.* **2009**, *131*, 7940−7941.

(4) Wallin, S.; Monnereau, C.; Blart, E.; Gankou, J.-R.; Odobel, F.; Hammarström, L. State-Selective Electron Transfer in an Unsymmetric Acceptor−Zn(II)porphyrin−Acceptor Triad: Toward a Controlled Directionality of Electron Transfer from the Porphyrin S2 and S1 States as a Basis for a Molecular Switch. *J. Phys. Chem. A* **2010**, *114*, 1709−1721.

(5) Bouit, P.-A.; Spänig, F.; Kuzmanich, G.; Krokos, E.; Oelsner, C.; Garcia-Garibay, M. A.; Delgado, J. L.; Martín, N.; Guldi, D. M. Efficient Utilization of Higher-Lying Excited States to Trigger Charge-Transfer Events. *Chem. - Eur. J.* **2010**, *16*, 9638−9645.

(6) Yushchenko, D. A.; Shvadchak, V. V.; Klymchenko, A. S.; Duportail, G.; Pivovarenko, V. G.; Mély, Y. Modulation of Excited-State Intramolecular Proton Transfer by Viscosity in Protic Media. *J. Phys. Chem. A* **2007**, *111*, 10435−10438.

(7) Rajendiran, N.; Balasubramanian, T. Dual Fluorescence of N-phenylanthranilic Acid: Effect of Solvents, pH and *β*-cyclodextrin. *Spectrochim. Acta, Part A* **2007**, *68*, 867−876.

(8) Glazer, E. C.; Magde, D.; Tor, Y. Dual Emission from a Family of Conjugated Dinuclear RuII Complexes. *J. Am. Chem. Soc.* **2005**, *127*, 4190−4192.

(9) Dantus, M.; Lozovoy, V. V. Experimental Coherent Laser Control of Physicochemical Processes. *Chem. Rev.* **2004**, *104*, 1813−1860.

(10) Luo, S.; Zhang, E.; Su, Y.; Cheng, T.; Shi, C. A Review of NIR Dyes in Cancer Targeting and Imaging. *Biomaterials* **2011**, *32*, 7127−7138.

(11) Guarin, C. A.; Villabona-Monsalve, J. P.; López-Arteaga, R.; Peon, J. Dynamics of the Higher Lying Excited States of Cyanine Dyes. An Ultrafast Fluorescence Study. *J. Phys. Chem. B* **2013**, *117*, 7352−7362.

(12) Müller, A.; Pflüger, E. Laser-Fashspectroscopy of Cryptocyanine. *Chem. Phys. Lett.* **1968**, *2*, 155−159.

(13) Tashiro, H.; Yajima, T. Direct Measurement of Blue Fluorescence Lifetimes in Polymethine Dyes Using a Picosecond Laser. *Chem. Phys. Lett.* **1976**, *42*, 553−557.

(14) Rěhák, V.; Novák, A.; Titz, M. S2 → S0 Fluorescence of cryptocyanine solutions. *Chem. Phys. Lett.* **1977**, *52*, 39−42.

(15) Das, D. K.; Makhal, K.; Singhal, S.; Goswami, D. Polarization Induced Control of Multiple Fluorescence from a Molecule. *Chem. Phys. Lett.* **2013**, *579*, 45−50.

(16) Kasatani, K.; Sato, H. Viscosity-Dependent Decay Dynamics of the S2 State of Cyanine Dyes with 3, 5, and 7 Methine Units by Picosecond Fluorescence Lifetime Measurements. *Bull. Chem. Soc. Jpn.* **1996**, *69*, 3455−3460.

(17) Nibbering, E. T. J.; Wiersma, D. A.; Duppen, K. Ultrafast Nonlinear Spectroscopy with Chirped Optical Pulses. *Phys. Rev. Lett.* **1992**, *68*, 514−517.

(18) Cerullo, G.; Bardeen, C. J.; Wang, Q.; Shank, C. V. High-Power Femtosecond Chirped Pulse Excitation of Molecules in Solution. *Chem. Phys. Lett.* **1996**, *262*, 362−368.

(19) Pastirk, I.; Brown, E. J.; Zhang, Q.; Dantus, M. Quantum Control of the Yield of a Chemical Reaction. *J. Chem. Phys.* **1998**, *108*, 4375−4378.

(20) Consani, C.; Ruetzel, S.; Nuernberger, P.; Brixner, T. Quantum Control Spectroscopy of Competing Reaction Pathways in a Molecular Switch. *J. Phys. Chem. A* **2014**, *118*, 11364−11372.

(21) Bardeen, C. J.; Yakovlev, V. V.; Squier, J. A.; Wilson, K. R. Quantum Control of Population Transfer in Green Fluorescent Protein by Using Chirped Femtosecond Pulses. *J. Am. Chem. Soc.* **1998**, *120*, 13023−13027.

(22) Fainberg, B. D. Nonperturbative Analytic Approach to the Interaction of Intense Ultrashort Chirped Pulses with Molecules in Solution: Picture of "Moving" Potentials. *J. Chem. Phys.* **1998**, *109*, 4523−4532.

(23) Bardeen, C. J.; Cao, J.; Brown, F. L. H.; Wilson, K. R. Using Time-dependent Rate Equations to Describe Chirped Pulse Excitation in Condensed Phases. *Chem. Phys. Lett.* **1999**, *302*, 405−410.

(24) Hashimoto, N. T.; Misawa, K.; Lang, R. Three-level Picture for Chirp-dependent Fluorescence Yields under Femtosecond Optical Pulse Irradiation. *Appl. Phys. Lett.* **2003**, *82*, 2749−2751.

(25) Fainberg, B. D.; Gorbunov, V. A. Coherent population transfer in molecules coupled with a dissipative environment by intense ultrashort chirped pulse. II. A simple model. *J. Chem. Phys.* **2004**, *121*, 8748−8754.

(26) Konar, A.; Lozovoy, V. V.; Dantus, M. Solvation Stokes-Shift Dynamics Studied by Chirped Femtosecond Laser Pulses. *J. Phys. Chem. Lett.* **2012**, *3*, 2458−2464.
(27) Herek, J. L.; Wohlleben, W.; Cogdell, R. J.; Zeidler, D.; Motzkus, M. Quantum control of energy flow in light harvesting. *Nature* **2002**, *417*, 533−535.
(28) Vogt, G.; Krampert, G.; Niklaus, P.; Nuernberger, P.; Gerber, G. Optimal Control of Photoisomerization. *Phys. Rev. Lett.* **2005**, *94*, 068305.
(29) Prokhorenko, V. I.; Nagy, A. M.; Waschuk, S. A.; Brown, L. S.; Birge, R. R.; Miller, R. J. D. Coherent Control of Retinal Isomerization in Bacteriorhodopsin. *Science* **2006**, *313*, 1257−1261.
(30) Vogt, G.; Nuernberger, P.; Brixner, T.; Gerber, G. Femtosecond pump−shaped-dump quantum control of retinal isomerization in bacteriorhodopsin. *Chem. Phys. Lett.* **2006**, *433*, 211−215.
(31) Buckup, T.; Lebold, T.; Weigel, A.; Wohlleben, W.; Motzkus, M. Singlet versus triplet dynamics of β-carotene studied by quantum control spectroscopy. *J. Photochem. Photobiol., A* **2006**, *180*, 314−321.
(32) Kuroda, D. G.; Singh, C. P.; Peng, Z.; Kleiman, V. D. Mapping Excited-State Dynamics by Coherent Control of a Dendrimer's Photoemission Efficiency. *Science* **2009**, *326*, 263−267.
(33) Schneider, J.; Wollenhaupt, M.; Winzenburg, A.; Bayer, T.; Kohler, J.; Faust, R.; Baumert, T. Efficient and robust strong-field control of population transfer in sensitizer dyes with designed femtosecond laser pulses. *Phys. Chem. Chem. Phys.* **2011**, *13*, 8733−8746.
(34) Sukharev, M.; Seideman, T. Optimal Control Approach to Suppression of Radiationless Transitions. *Phys. Rev. Lett.* **2004**, *93*, 093004.
(35) Abe, M.; Ohtsuki, Y.; Fujimura, Y.; Domcke, W. Optimal control of ultrafast cis-trans photoisomerization of retinal in rhodopsin via a conical intersection. *J. Chem. Phys.* **2005**, *123*, 144508.
(36) Hunt, P. A.; Robb, M. A. Systematic Control of Photochemistry: The Dynamics of Photoisomerization of a Model Cyanine Dye. *J. Am. Chem. Soc.* **2005**, *127*, 5720−5726.
(37) Petersen, J.; Wohlgemuth, M.; Sellner, B.; Bonacic-Koutecky, V.; Lischka, H.; Mitric, R. Laser pulse trains for controlling excited state dynamics of adenine in water. *Phys. Chem. Chem. Phys.* **2012**, *14*, 4687−4694.
(38) Brixner, T.; Gerber, G. Quantum Control of Gas-Phase and Liquid-Phase Femtochemistry. *ChemPhysChem* **2003**, *4*, 418−438.
(39) Wohlleben, W.; Buckup, T.; Herek, J. L.; Motzkus, M. Coherent Control for Spectroscopy and Manipulation of Biological Dynamics. *ChemPhysChem* **2005**, *6*, 850−857.
(40) Lozovoy, V. V.; Pastirk, I.; Dantus, M. Multiphoton Intrapulse Interference. IV. Ultrashort Laser Pulse Spectral Phase Characterization and Compensation. *Opt. Lett.* **2004**, *29*, 775−7.
(41) Coello, Y.; Lozovoy, V. V.; Gunaratne, T. C.; Xu, B.; Borukhovich, I.; Tseng, C.-h.; Weinacht, T.; Dantus, M. Interference Without an Interferometer: a Different Approach to Measuring, Compressing, and Shaping Ultrashort Laser Pulses. *J. Opt. Soc. Am. B* **2008**, *25*, A140−A150.
(42) Devi, P.; Lozovoy, V. V.; Dantus, M. Measurement of Group Velocity Dispersion of Solvents Using 2-cycle Femtosecond Pulses: Experiment and Theory. *AIP Adv.* **2011**, *1*, 032166.
(43) Strekowski, L.; Lipowska, M.; Patonay, G. Substitution reactions of a nucleofugal group in heptamethine cyanine dyes. Synthesis of an isothiocyanato derivative for labeling of proteins with a near-infrared chromophore. *J. Org. Chem.* **1992**, *57*, 4578−4580.
(44) West, W.; Pearce, S. The Dimeric State of Cyanine Dyes. *J. Phys. Chem.* **1965**, *69*, 1894−1903.
(45) Yu, A.; Tolbert, C. A.; Farrow, D. A.; Jonas, D. M. Solvatochromism and Solvation Dynamics of Structurally Related Cyanine Dyes. *J. Phys. Chem. A* **2002**, *106*, 9407−9419.
(46) Webster, S.; Padilha, L. A.; Hu, H.; Przhonska, O. V.; Hagan, D. J.; Van Stryland, E. W.; Bondar, M. V.; Davydenko, I. G.; Slominsky, Y. L.; Kachkovski, A. D. Structure and linear spectroscopic properties of near IR polymethine dyes. *J. Lumin.* **2008**, *128*, 1927−1936.
(47) Bricks, J. L.; Kachkovskii, A. D.; Slominskii, Y. L.; Gerasov, A. O.; Popov, S. V. Molecular design of near infrared polymethine dyes: A review. *Dyes Pigm.* **2015**, *121*, 238−255.
(48) Grabowski, Z. R.; Rotkiewicz, K.; Rettig, W. Structural Changes Accompanying Intramolecular Electron Transfer: Focus on Twisted Intramolecular Charge-Transfer States and Structures. *Chem. Rev.* **2003**, *103*, 3899−4032.
(49) Zhang, Z.; Berezin, M. Y.; Kao, J. L. F.; d'Avignon, A.; Bai, M.; Achilefu, S. Near-Infrared Dichromic Fluorescent Carbocyanine Molecules. *Angew. Chem., Int. Ed.* **2008**, *47*, 3584−3587.
(50) Passino, S. A.; Nagasawa, Y.; Joo, T.; Fleming, G. R. Three-Pulse Echo Peak Shift Studies of Polar Solvation Dynamics. *J. Phys. Chem. A* **1997**, *101*, 725−731.
(51) Mohanty, J.; Palit, D. K.; Mittal, J. P. Photophysical Properties of Two Infrared Laser dyes - IR-144 and IR-140: A Picosecond Laser Flash Photolysis Study. *Proc. Indian Nat. Sci. Acad. Part A* **2000**, *66*, 303−315.
(52) Carson, E. A.; Diffey, W. M.; Shelly, K. R.; Lampa-Pastirk, S.; Dillman, K. L.; Schleicher, J. M.; Beck, W. F. Dynamic-Absorption Spectral Contours: Vibrational Phase-Dependent Resolution of Low-Frequency Coherent Wave-Packet Motion of IR144 on the Ground-State and Excited-State $\pi \rightarrow \pi^*$ Surfaces. *J. Phys. Chem. A* **2004**, *108*, 1489−1500.
(53) Konar, A.; Lozovoy, V. V.; Dantus, M. Solvent Environment Revealed by Positively Chirped Pulses. *J. Phys. Chem. Lett.* **2014**, *5*, 924−928.
(54) Nairat, M.; Konar, A.; Kaniecki, M.; Lozovoy, V. V.; Dantus, M. Investigating the Role of Human Serum Albumin Protein Pocket on the Excited State Dynamics of Indocyanine Green Using Shaped Femtosecond Laser Pulses. *Phys. Chem. Chem. Phys.* **2015**, *17*, 5872−5877.
(55) Gunaratne, T. C.; Zhu, X.; Lozovoy, V. V.; Dantus, M. Symmetry of Nonlinear Optical Response to Time Inversion of Shaped Femtosecond Pulses as a Clock of Ultrafast Dynamics. *Chem. Phys.* **2007**, *338*, 259−267.
(56) Sanchez-Galvez, A.; Hunt, P.; Robb, M. A.; Olivucci, M.; Vreven, T.; Schlegel, H. B. Ultrafast Radiationless Deactivation of Organic Dyes: Evidence for a Two-State Two-Mode Pathway in Polymethine Cyanines. *J. Am. Chem. Soc.* **2000**, *122*, 2911−2924.
(57) Bishop, M. M.; Roscioli, J. D.; Ghosh, S.; Mueller, J. J.; Shepherd, N. C.; Beck, W. F. Vibrationally Coherent Preparation of the Transition State for Photoisomerization of the Cyanine Dye Cy5 in Water. *J. Phys. Chem. B* **2015**, *119*, 6905−6915.
(58) Freed, K. F.; Jortner, J. Multiphonon Processes in the Nonradiative Decay of Large Molecules. *J. Chem. Phys.* **1970**, *52*, 6272−6291.
(59) Boyd, R. *Nonlinear Optics*; Academic Press: Burlington, 2008.
(60) Migani, A.; Olivucci, M. Conical Intersections and Organic Reaction Mechanisms. In *Conical Intersections: Electronic Structure, Dynamics & Spectroscopy*; World Scientific: Singapore, 2004; pp 271−320.
(61) Sampedro Ruiz, D.; Cembran, A.; Garavelli, M.; Olivucci, M.; Fuß, W. Structure of the Conical Intersections Driving the *cis*−*trans* Photoisomerization of Conjugated Molecules. *Photochem. Photobiol.* **2002**, *76*, 622−633.
(62) Pollard, W. T.; Lee, S.-Y.; Mathies, R. A. Wave Packet Theory of Dynamic Absorption Spectra in Femtosecond Pump−probe Experiments. *J. Chem. Phys.* **1990**, *92*, 4012−4029.
(63) Pollard, W. T.; Mathies, R. A. Analysis of Femtosecond Dynamic Absorption Spectra of Nonstationary States. *Annu. Rev. Phys. Chem.* **1992**, *43*, 497−523.
(64) Scherer, N. F.; Jonas, D. M.; Fleming, G. R. Femtosecond Wave Packet and Chemical Reaction Dynamics of Iodine in Solution: Tunable Probe Study of Motion Along the Reaction Coordinate. *J. Chem. Phys.* **1993**, *99*, 153−168.
(65) Jonas, D. M.; Bradforth, S. E.; Passino, S. A.; Fleming, G. R. Femtosecond Wavepacket Spectroscopy: Influence of Temperature, Wavelength, and Pulse Duration. *J. Phys. Chem.* **1995**, *99*, 2594−2608.

DOI: 10.1021/acs.jpca.6b01835
J. Phys. Chem. A 2016, 120, 1876−1885

(66) Kim, J.; Mukamel, S.; Scholes, G. D. Two-dimensional Electronic Double-quantum Coherence Spectroscopy. *Acc. Chem. Res.* **2009**, *42*, 1375−1384.
(67) Weidinger, D.; Engel, M. F.; Gruebele, M. Freezing Vibrational Energy Flow: A Fitness Function for Interchangeable Computational and Experimental Control. *J. Phys. Chem. A* **2009**, *113*, 4184−4191.
(68) Tomasi, J.; Mennucci, B.; Cammi, R. Quantum Mechanical Continuum Solvation Models. *Chem. Rev.* **2005**, *105*, 2999−3094.
(69) Polívka, T.; Sundström, V. Ultrafast Dynamics of Carotenoid Excited States−From Solution to Natural and Artificial Systems. *Chem. Rev.* **2004**, *104*, 2021−2072.

DOI: 10.1021/acs.jpca.6b01835
J. Phys. Chem. A 2016, 120, 1876−1885